Morphological Attribute Profiles for the Analysis of Very High Resolution Images

Mauro Dalla Mura, *Student Member, IEEE*, Jón Atli Benediktsson, *Fellow, IEEE*, Björn Waske, *Member, IEEE*, and Lorenzo Bruzzone, *Fellow, IEEE*

***Abstract*—Morphological attribute profiles (APs) are defined as a generalization of the recently proposed morphological profiles (MPs). APs provide a multilevel characterization of an image created by the sequential application of morphological attribute filters that can be used to model different kinds of the structural information. According to the type of the attributes considered in the morphological attribute transformation, different parametric features can be modeled. The generation of APs, thanks to an efficient implementation, strongly reduces the computational load required for the computation of conventional MPs. Moreover, the characterization of the image with different attributes leads to a more complete description of the scene and to a more accurate modeling of the spatial information than with the use of conventional morphological filters based on a predefined structuring element. Here, the features extracted by the proposed operators were used for the classification of two very high resolution panchromatic images acquired by Quickbird on the city of Trento, Italy. The experimental analysis proved the usefulness of APs in modeling the spatial information present in the images. The classification maps obtained by considering different APs result in a better description of the scene (both in terms of thematic and geometric accuracy) than those obtained with an MP.**

***Index Terms*—Classification, mathematical morphology, morphological attribute profiles (APs), morphological profiles (MPs), object detection, remote sensing, very high resolution (VHR) images.**

I. Introduction

HIGH spatial resolution in the latest generation of optical sensors such as Ikonos, QuickBird, Spot-5, and Worldview (up to 0.5 m) has increased the range of applications where remote sensing (RS) data can be usefully employed. The great amount of thematic information contained in very high resolution (VHR) images can be exploited in tasks addressing the analysis of land cover/use and object extraction. In particular, VHR imagery is very useful for investigating urban environments (e.g., in urban growth planning and monitoring, road network map-updating, discovering building abuse, etc.) where a detailed representation of the scene can significantly improve the results of the analysis with respect to low-resolution data (like those acquired by Landsat Thematic Mapper and Enhanced Thematic Mapper Plus). For example, fine representation of details in a scene can be exploited in object detection tasks, where the characterization of the geometrical features of objects is of fundamental importance.

The technical features of VHR data require the development of specific methods for data analysis. For example, the contextual spectral similarity of connected pixels is a fundamental property of VHR data, whereas, it is less relevant in medium-resolution images. Furthermore, the fine representation of geospatial objects and the great amount of details improve the representation of the surveyed scene but, at the same time, significantly increase the complexity of VHR images, leading to a substantial difficulty in extracting the relevant informative components according to automatic analysis procedures. The great heterogeneity of the imaged scene (e.g., the same thematic objects might appear either as homogeneous or highly textured regions in the image), due to the high resolution of the sensor, cannot be handled by general image processing techniques developed for medium/high-resolution sensors. Moreover, the increased geometrical resolution leads on the one hand to a fine representation of the scene, whereas, to the other hand to a decreased resolution in the spectral domain which further increases the spectral ambiguity of different land-cover types. This results in a reduction of the effectiveness of conventional classification methodologies based on the analysis of spectral features [1]. Thus, features that can be used effectively to model the spatial information of the pixels by exploiting contextual relations must be included in the analysis of VHR data.

Several techniques specifically developed for incorporating information extracted by modeling the spatial properties in analysis of VHR images have been presented in the literature. Usually, information extracted from the spatial characteristics of the image is combined with the available spectral features in the analysis. The spatial information can be extracted through the application of filters by performing a contextual image transformation, i.e., an image mapping that transforms a pixel as a function of the values of a set of pixels (usually its neighbors). In most cases, the transformation reduces, in some ways, the complexity of the scene by attenuating some details. The outcome of the transformation depends on how the structures that are present in the image interact with the neighborhood of the filter. Since, particularly in VHR images, the shapes and contours of the regions are perceptually very

Manuscript received October 3, 2009; revised December 3, 2009. Date of publication June 7, 2010; date of current version September 24, 2010.

M. Dalla Mura is with the Department of Information Engineering and Computer Science, University of Trento, 38123 Trento, Italy and also with the Faculty of Electrical and Computer Engineering, University of Iceland, 101 Reykjavik, Iceland (e-mail: dallamura@disi.unitn.it).

J. A. Benediktsson is with the Faculty of Electrical and Computer Engineering, University of Iceland, 101 Reykjavik, Iceland (e-mail: benedikt@hi.is).

B. Waske is with the Institute of Geodesy and Geoinformation, Department of Photogrammetry, University of Bonn, 53115 Bonn, Germany (e-mail: bwaske@uni-bonn.de).

L. Bruzzone is with the Department of Information Engineering and Computer Science, University of Trento, 38123 Povo, Italy (e-mail: lorenzo.bruzzone@ing.unitn.it).

Color versions of one or more of the figures in this paper are available online at http://ieeexplore.ieee.org.

Digital Object Identifier 10.1109/TGRS.2010.2048116

significant, the filtering technique should simultaneously attenuate the unimportant details and preserve the geometrical characteristics of the other regions. This property is elegantly achieved by morphological connected filters, such as filters by reconstruction [2]. For instance, openings and closings by reconstruction can suppress brighter and darker regions (with respect to the graylevel of the adjacent regions), respectively, that are smaller than the moving window used in the transformation [which is called structuring element (SE)]. On the contrary, the structures that are larger than the SE are completely preserved, leaving their geometry unaffected. The SE, which specifies the neighborhood considered for each pixel and the morphological operator, defines the amount of contextual relations included in the analysis. Pesaresi and Benediktsson [3] introduced the application of this family of filters to VHR images. They performed a multiscale analysis by computing an anti-granulometry and a granulometry, (i.e., a sequence of closings and openings of increasing size), appended in a common data structure called morphological profile [3]. The derivative of the morphological profile (DMP), which shows the residues of two successive filtering operations (i.e., two adjacent levels in the profile), was exploited for classifying VHR panchromatic images and for the definition of a novel segmentation technique. The obtained segmentation map, called morphological characteristic, is generated by associating each pixel to the level where the maximum of the DMP (evaluated at the given pixel) occurs. Since their definition, MPs and DMPs have been widely used for the analysis of remote sensing images. In [4], the MP generated by standard opening and closing was computed on a Quickbird panchromatic image acquired on an area hit by the 2003 Bam earthquake. The spatial features extracted by the MP were used for assessing the damages caused by the earthquake. Recently, the standard morphological operators of opening, closing, white, and black top hat, along with opening and closing by reconstruction, were used together with support vector machines for the classification of a Quickbird panchromatic image, [5]. An automatic hierarchical segmentation technique based on the analysis of the DMP was proposed in [6]. The segmentation process is performed according to a criterion based on the spectral homogeneity and spatial connectedness computed on the segments extracted by the DMP at each level. The DMP was also analyzed in [7], by extracting a fuzzy measure of the characteristic scale and contrast of each structure in the image. The computed measures were compared with the possibility distribution predefined for each thematic class, generating a value of membership degree for each class used for classification. In [8], feature extraction techniques were applied to the DMP in order to reduce the dimensionality of the features considered by a neural network classifier. In [9], the analysis based on MPs was successfully extended to the processing of hyperspectral high-resolution images, by computing the MPs on the principal components of the data [which were called extended morphological profiles (EMPs)]. Since the EMP do not fully exploit the spectral information, in [10], they were considered along with the original hyperspectral data by a support vector machines for classification.

As can be observed from the aforementioned literature, the computation of a multiscale processing (e.g., by MPs, DMPs, EMPs) has proven to be effective in extracting informative spatial features from the analyzed images. For example, MPs computed with a compact SE (e.g., square, disk, etc.) can be used for modeling the size of the objects in the image (e.g., in [10] this information was exploited for discriminating small buildings from large ones). Recently, the computation of two MPs was proposed for modeling both the length and the width of the structures [11]. In greater detail, one MP is built by disk-shaped SEs for extracting the smallest size of the structures, while the other employs linear SEs (which generate directional profiles [12]) for characterizing the objects maximum size (along the orientation of the SE). This is useful for defining the minimal and maximal length but, as all the possible lengths and orientations cannot be practically investigated, such analysis is computationally intensive. Nevertheless, as proven in [13], filters by reconstruction are suitable for handling the geometrical information of the scene. This was observed by applying filters by reconstruction in order to reduce the image complexity for change detection on VHR images. In [14], we introduced the use of morphological attribute filters for VHR remote sensing images, as an extension of the common morphological filters by reconstruction based on SEs. These operators are morphological connected filters. Thus, they process the image without distorting or inserting new edges but only by merging existing flat regions [2]. Attribute filters were employed for modeling the structural information of the scene for classification and building extraction in [14] and [15], respectively, where they proved to be suitable for the modeling of structural information in VHR images. Attribute filters include in their definition, the morphological operators based on geodesic reconstruction [16]. Moreover, they are a flexible tool since they can perform a processing based on many different types of attributes. In fact, the attributes can be of any type. For example, they can be purely geometric, or related to the spectral values of the pixels, or on different characteristics. Furthermore, in [15], the problem of the tuning of the parameters of the filter was addressed by proposing an automatic selection procedure based on a genetic algorithm.

In this paper, we propose to characterize the spatial information of VHR data by using a multilevel, multi-attribute approach based on morphological attribute filters. In particular, this paper aims at extending the works in [14] and [15] by presenting a formal definition of morphological attribute profiles and differential attribute profiles. These are proposed to be an extension of the morphological profiles and of their derivative concepts, which are conventionally defined for openings and closings by reconstruction. Thus, the proposed theoretical framework permits the definition of a more general set of profiles based on the morphological attribute operators. The profiles built by morphological attribute filters permit a more flexible investigation of the scene, leading to a better modeling of the spatial information. Moreover, thanks to an efficient implementation, their application becomes computationally less demanding than conventional profiles built with operators by reconstruction.

The paper is organized in six sections. The next section recalls and discusses the concept of morphological profiles. Section III introduces morphological attribute filters theory. In Section IV, attribute profiles are formally defined. Section V presents the results of the experimental analysis carried out for

assessing the effectiveness of the proposed operators in modeling the spatial information. Finally, conclusions are drawn in Section VI.

II. Background on Morphological Profiles

In this section, we introduce the concepts of morphological profiles and differential morphological profiles following the presentation given in [3]. This leads us to investigate how the profiles are computed in order to point out the related limitations. In the following, we recall some useful definitions for the next discussion.

A. Definitions

A binary image F is a mapping of the subset E, of the image domain $\mathbb{R}^n$ or $\mathbb{Z}^n$ (usually $n = 2$, i.e., 2-D images) into the couple $\{0, 1\}$. A grayscale image f (with single tone values) is a mapping from E to $\mathbb{R}$ or $\mathbb{Z}$. Here, we follow the arbitrary convention of assigning capital letters to binary variables and binary transformations, whereas small caps refer to grayscale images and mappings.

A *connected component* X of a binary image (in [17] also called a *grain*) is a set of pixels in which each pair of pixels is connected. Two pixels are connected according to a connectivity rule. The iso-intensity connected components of a grayscale image are called *flat zones*. Common connectivity rules are the four- and eight-connected, where a pixel is said to be adjacent to four or eight of its neighboring pixels, respectively. The connectivity can be extended by more general criteria defining a connectivity class [18].

A *criterion* T is a mapping of a generic set S to the couple of Booleans $\{\text{false}, \text{true}\}$.

An image transformation ψ is a mapping from E to E with $\psi(f) \to \mathbb{R}$ or $\mathbb{Z}$ in the grayscale case. We recall some properties of an image transformation ψ:

- Increasingness: $\psi(f) \leq \psi(g)$ if $f \leq g \; \forall f, g \in E$
- Anti-extensivity: $\psi(f) \leq f$
- Extensivity: $\psi(f) \geq f$
- Idempotence: $\psi\psi = \psi$
- Absorption property: $\psi_i\psi_j = \psi_i\psi_j = \psi_{\max(i,j)}$.

B. Morphological Profiles

Let us first consider an opening by reconstruction, $\gamma_R^i(f)$, applied to an image f with an SE of size i. The opening by reconstruction can be computed as a sequence of an erosion with the SE followed by a reconstruction by dilation [2]. By duality, a closing by reconstruction, $\phi_R^i(f)$, is defined as the dilation of the original image with SE of size i, followed by a geodesic reconstruction by erosion [2]. The geodesic reconstruction, either by dilation or by erosion, is an iterative procedure that is performed until idempotence is reached.

When opening by reconstruction is computed on the image with an SE of increasing size, we obtain a *morphological opening profile* which can be formalized as

$$\Pi_{\gamma_R}(f) = \left\{\Pi_{\gamma\lambda} : \Pi_{\gamma\lambda} = \gamma_R^\lambda(f), \forall\lambda \in [0, \ldots, n]\right\}. \quad (1)$$

This leads to perform a multiscale analysis of the image.

According to its definition, the opening profile is a granulometry built by openings by reconstruction, which is defined in the mathematical morphology framework as a family of idempotent, anti-extensive and increasing transformations (i.e., openings) that fulfill the absorption property [2]. Analogously, a *morphological closing profile* is defined as

$$\Pi_{\phi_R}(f) = \left\{\Pi_{\phi\lambda} : \Pi_{\phi\lambda} = \phi_R^\lambda(f), \forall\lambda \in [0, \ldots, n]\right\}. \quad (2)$$

The closing profile is an anti-granulometry generated by closings by reconstruction.

When the size, λ, of the SE is zero, then $\prod_{\gamma^0}(f) = \prod_{\phi^0}(f)$ holds, corresponding to the original image f.

A morphological profile, generated by geodesic operators, is simply the concatenation of closing and opening profiles, as shown in (3) at the bottom of the page. The resulting MP is a stack of $2n + 1$ images (n images from the closing profile, the original image and n images from the opening profile). By computing the derivative of a MP, a *differential morphological profile* is generated, as shown in (4) at the bottom of the page. Above the differential opening profile, Δ_γ, and the differential closing profile, Δ_ϕ, are respectively defined as

$$\Delta_{\gamma_R}(f) = \left\{\Delta_{\gamma\lambda} : \Delta_{\gamma\lambda} = \Pi_{\gamma(\lambda-1)} - \Pi_{\gamma\lambda}, \forall\lambda \in [1, n]\right\} \quad (5)$$

$$\Delta_{\phi_R}(f) = \left\{\Delta_{\phi\lambda} : \Delta_{\phi\lambda} = \Pi_{\phi\lambda} - \Pi_{\phi(\lambda-1)}, \forall\lambda \in [1, n]\right\}. \quad (6)$$

As seen from (4), the DMP stores the residuals of the subsequent increasing transformations applied to the image. This might be more practical with respect to the MPs for analyzing the output of the multiscale analysis since the most important components of the profiles are more evident in the DMP.

$$\Pi(f) = \left\{\Pi_i : \left\langle \begin{array}{lll} \Pi_i = \Pi_{\phi\lambda}, & \text{with } \lambda = (n - i + 1), & \forall i \in [1, n] \\ \Pi_i = \Pi_{\gamma\lambda}, & \text{with } \lambda = (i - n - 1), & \forall i \in [n + 1, 2n + 1] \end{array} \right.\right\} \quad (3)$$

$$\Delta(f) = \left\{\Delta_i : \left\langle \begin{array}{lll} \Delta_i = \Delta_{\phi\lambda}, & \text{with } \lambda = (n - i + 1), & \forall i \in [1, n] \\ \Delta_i = \Delta_{\gamma\lambda}, & \text{with } \lambda = (i - n), & \forall i \in [n + 1, 2n] \end{array} \right.\right\} \quad (4)$$

C. Limitations of Morphological Profiles

The main limitation of MPs lies in the partial analysis that is performed with the computation of the profile. In greater detail, MPs attempt to model the spatial information within the scene by analyzing the interaction of a set of SEs of fixed shape and increasing size with the objects in the image. Although this is a powerful tool for performing an investigation on the scale of the structures (thanks to the suitability of the SEs for modeling the size of the objects), it leads only to a partial characterization of the objects in the scene. In fact, one could aim at a description of the image based on other features (e.g., shape, texture, etc.) rather than the size in order to increase the discriminative power of the analysis. From a theoretical viewpoint, filters by reconstruction based on SEs could be used to model other geometrical features, e.g., to represent the information on the shape of the regions by analyzing a set of MPs generated by SEs of different shapes. Nonetheless, the generation of profiles for different shapes would be computationally unfeasible. In fact, in order to perform an analysis aimed at modeling the shape characteristic, the range of the possible sizes assumed by all the components in the image should be investigated by each profile in order to remove the dependence of the results to the scale.

Another important limitation is the strong constraint given by the use of a SE for modeling the concepts of different characteristics of the spatial information (e.g., size, shape, homogeneity, etc.). This limitation is particularly evident when features more complex than the geometrical primitives of size and shape are required (e.g., shape factor, length of the skeleton of a region, etc.). Moreover, SEs are intrinsically unsuitable to describe features related to the gray-level characteristics of the regions (e.g., spectral homogeneity, contrast, etc.).

A final limitation of MPs is the computational complexity associated with their generation. The original image has to be completely processed for each level of the profile, which requires two complete processing of the image; one performed by a closing and the other by an opening transformation. Thus, the complexity increases linearly with the number of levels included in the profile.

III. Morphological Attribute Filters

Morphological attribute openings and attribute thinnings (called attribute filters) are morphological adaptive filters introduced by Breen and Jones [16]. For simplicity, we introduce these operators for the binary case and later, we extend the concepts to the grayscale. The discussion will be focused first on opening and thinning. Then, the results are reported analogously for closing and thickening.

A. Binary Attribute Operators

Binary attribute openings operate on connected components of a binary image according to an increasing criterion. The transformation removes all those connected components for which the criterion is not satisfied, leaving the others unaffected. In order to introduce their formal definition, the binary connected opening and binary trivial opening have to be defined.

Binary connected opening, Γ_x, transforms a binary image f given a pixel x, by keeping the connected component that contains x and removing all the others. *Binary trivial opening* Γ_T operates on a given connected component X according to an increasing criterion T applied to the connected component. If the criterion is satisfied, the connected component is preserved, otherwise it is removed according to

$$\Gamma_T(X) = \begin{cases} X, & \text{if } T(X) = true \\ 0, & \text{if } T(X) = false. \end{cases} \tag{7}$$

In general, one or more features of the connected component, on which the filter is applied, are compared to a given threshold defined by the rule. If a criterion T is increasing, then, if it is satisfied for a connected component X, it will be also satisfied by all the regions that enclose X (i.e., the superset of X). Formally for $X \subseteq Y$, $T(X) \subseteq T(Y)$. Examples of increasing criteria are the comparison to a reference value (λ) of the attributes computed on a region such as the area, the volume (sum of the graylevels of all the pixels belonging to the region), the size of the bounding box, etc. It is straightforward to prove that every region enclosing the one on which these criteria are computed will have attribute values that are greater or equal than the computed ones.

Binary attribute opening Γ^T, given an increasing criterion T, is defined as a binary trivial opening applied on all the connected components of F. This can be formally represented as

$$\Gamma^T(F) = \bigcup_{x \in F} \Gamma_T \left[\Gamma_x(F)\right]. \tag{8}$$

If the criterion evaluated in the transformation is not increasing, e.g., when the computed attribute is not dependent itself on the scale of the regions (e.g., shape factor, orientation, homogeneity, etc.), the transformation also becomes not increasing. Even if the increasingness property is not fulfilled, the filter remains idempotent and anti-extensive. For this reason, the transformation based on a non-increasing criterion is not an opening, but a thinning. Then, analogously to the definition of attribute openings, *binary attribute thinning* $\tilde{\Gamma}^T$ can be defined as

$$\tilde{\Gamma}^T(F) = \bigcup_{x \in F} \tilde{\Gamma}_T \left[\Gamma_x(F)\right] \tag{9}$$

where $\tilde{\Gamma}_T$ denotes a trivial thinning.

All the definitions above can be extended to the respective dual transformations. *Binary attribute closing* Φ^T.[1] Thus, defined as the binary union of the connected components that fulfill the criterion T

$$\Phi^T(F) = \bigcup_{x \in F} \Phi_T \left[\Phi_x(F)\right]. \tag{10}$$

This is based on the operators of Φ_T and Φ_X, respectively, binary trivial closing and *binary connected closing.*

[1] In contrast to [16], here Φ denotes a closing transformation.

Non-increasing attribute T, leads to a binary attribute thickening $\tilde{\Phi}^T$ given by

$$\tilde{\Phi}^T(F) = \bigcup_{x \in F} \tilde{\Phi}_T \left[\Phi_x(F)\right] \tag{11}$$

with $\tilde{\Phi}_T$ the binary trivial thickening.

B. Grayscale Attribute Operators

Attribute openings and thinnings introduced for the binary case can be extended to grayscale images employing the threshold decomposition principle [2]. A grayscale image can be represented by a stack of binary images obtained by thresholding the original image at each of its graylevels. Then, the binary attribute opening can be applied to each binary image and *the grayscale attribute opening* is given by the maximum graylevel of the results of the filtering for each pixel and can be mathematically presented as

$$\gamma^T(f)(x) = \max\left\{k : x \in \Gamma^T\left[Th_k(f)\right]\right\} \tag{12}$$

where $Th_k(f)$ is the binary image obtained by thresholding f at graylevel k (with k ranging on the graylevels of f).

The extension to grayscale of the binary attribute thinning is not straightforward and not unique. For example, a possible definition of a grayscale attribute thinning can be given analogously to (12) as:

$$\tilde{\gamma}^T(f)(x) = \max\left\{k : x \in \tilde{\Gamma}^T\left[Th_k(f)\right]\right\}. \tag{13}$$

However, other definitions are possible, according to the filtering rule considered in the analysis. A list of possible filtering rules is presented in Section III-C. If the criterion T is increasing, the result of the thinning is actually an opening transformation. In this case, (13) is equal to (12). Although, this approach does not lead to the fastest implementation of such operators, it permits a more direct link to the correspondent binary operators.

Attribute openings are a family of operators that also includes openings by reconstruction [16]. If we consider a binary image with a connected component X and the increasing criterion "the size of the largest square enclosed by X must be greater than λ," the result of the attribute opening is the same as applying an opening by reconstruction with a squared SE of size λ. The extension of this example to the grayscale case is straightforward. Given this correspondence between the criterion and the SE, we point out that any opening by reconstruction can be denoted and performed as attribute opening.

The concepts presented above are straightforwardly extended to closing/thickening leading to the definition of *grayscale attribute closing*, i.e.,

$$\phi^T(f)(x) = \min\left\{k : x \in \Phi^T\left[Th_k(f)\right]\right\} \tag{14}$$

and *grayscale attribute thickening*:

$$\tilde{\phi}^T(f)(x) = \min\left\{k : x \in \tilde{\Phi}^T\left[Th_k(f)\right]\right\}. \tag{15}$$

As for attribute thinning, other definitions are available according to the selected filtering rule. For an example of the effects of attribute filtering, the reader can refer to Fig. 2 (synthetic image) and Fig. 6 (real remote sensing image).

C. Max-Tree

The Max-tree data representation, introduced by Salembier *et al.* [19], is of particular interest because it increases the efficiency of the filtering by splitting the transformation process into three separate phases: 1) tree creation; 2) filtering; and 3) image restitution. These phases are presented in detail below.

1) *Max-tree creation.* For simplicity, let us initially consider a binary image F. It can be represented in a rooted tree structure with a depth of two. This is composed by a single root node, which represents the pixels of the background, and children nodes connected to the root, where each of them refers to a connected component (C_i) in F. The extension of the tree built for the binary case to the grayscale can be easily explained by the threshold decomposition of the image. The levels in the depth of the tree represent the graylevels of the image and at each level, the number of nodes corresponds to the number of connected components present in the binary image obtained by thresholding the current graylevel. The tree starts to grow from the root. The connected component of the root is given by thresholding the image at its lowest graylevel, thus representing the entire image domain, E. By increasing the value of the graylevel, the thresholded image will show separated connected components, represented by nodes at the level in the tree corresponding to the threshold. Those nodes are then linked to their parent nodes at the closest inferior level in the tree. In the image, each parent node corresponds to a connected component which is a superset of the connected component represented by the children node in the tree. The procedure is iterated until the threshold reaches the maximum graylevel of the image, which defines the leaves of the tree (the absolute maxima of the image).
2) *Filtering.* Once the tree is defined, the criterion associated with the transformation is evaluated at each node (i.e., the attribute is checked against a reference value λ). Subsequently, the tree is pruned by removing the nodes that do not satisfy the criterion according to a filtering rule. There are two typologies of filtering rules: 1) *pruning strategies*, which remove or preserve a node together with its descendants; and 2) *nonpruning strategies*, where if a node is removed, its children are linked to the parent of the removed node. Below we briefly discuss a few strategies. The Min, Max and the Viterbi decision rules [19] are pruning strategies, while the Direct and the Subtractive rules [20] are nonpruning strategies. In particular, the Subtractive rule proved to be particular useful when associated to attributes for describing the shapes of objects [21].
   - *Min*: If a node does not satisfy the criterion, then it is removed together with all its descendants;

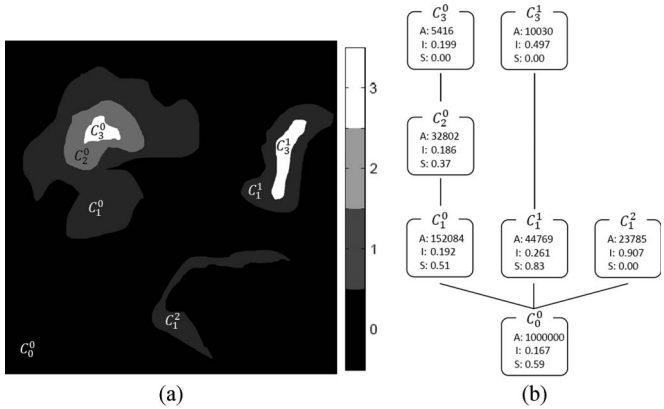

Fig. 1. Example of the Max-tree representation. (a) Input image and (b) Max-tree structure representing the connected components of the image. Each node reports also the values of three attributes: area (A), moment of inertia (I) and standard deviation (S).

- *Max*: A node that does not satisfy the criterion is suppressed, only if the criterion is not satisfied by all of its descendants.
- *Direct*: If a node does not satisfy the criterion, then it is removed by leaving unaffected all of its descendants that satisfy it.
- *Viterbi*: The nodes are removed by evaluating the costs associated with the decision and by taking the solution with the minimum cost.
- *Subtractive*: If a node does not satisfy the criterion, then it is removed and all its descendants are lowered by its gray level. A formal definition of the grayscale attribute thinning operator employing this filtering rule can be found in [21].

Again, if the criterion is increasing (i.e., the transformation is an opening), all the strategies lead to the same result.

3) *Image restitution.* The final phase of the transformation aims at converting back the pruned tree to an image. This is done by assigning to each pixel the graylevel correspondent to the highest level of the tree having a node whose correspondent connected component in the image encloses the pixel.

In Fig. 1(b), the Max-tree of a sample image of 1000×1000 pixels [Fig. 1(a)] is presented. On each connected component of the image (correspondent to a node in the tree), three attributes are computed. Fig. 2 shows the Max-tree of the image pruned according to different criteria and the correspondent filtered images. The attributes selected are: 1) area (related the size of the regions); 2) first moment invariant of Hu [22], also referred as "moment of inertia" (which models the elongation of the regions); and 3) standard deviation (which measures the homogeneity of the pixels enclosed by the regions). The first moment invariant of Hu can be associated to the moment of inertia in kinematics because it measures the spread of a region with respect to its center of mass [22]. The moment of inertia attribute is a measure of the noncompactness of the objects, since it has small values for compact regions, while rapidly increases for the elongated ones [23].

The flexibility of the attribute selection makes these filters appealing with respect to traditional opening and closing by reconstruction based on SEs, since any attribute that can be computed on the regions of the image can be selected for the analysis. As an example, some attributes that can be interesting for the analysis of remote sensing images are area, volume (sum of the intensities of the pixels belonging to each region), length of the diagonal of the box bounding each region, moment of inertia, shape factor, simplicity and complexity of the regions [19], homogeneity, standard deviation, and entropy of the grayscale values of the pixels. Other examples of attributes used by attribute filters can be found in [16] and other regional descriptors that can be used as attributes can be found in [23].

The separation of the computation of the attributes and the filtering phase results in another advantage of this filtering architecture over the application of conventional operators by reconstruction. In fact, since the value of the attributes is computed on all the regions before the filtering phase, it is possible to avoid defining λ, the threshold value checked by the criterion, for values that are not significant (e.g., out of the range of the real values of the attributes).

IV. Morphological Attribute Profiles[2]

In this section, we introduce the concepts of *attribute profiles* (APs) and *differential attribute profiles* (DAPs). These multilevel filters are based on morphological attribute operators and they are a generalization of the conventional MPs and DMPs discussed in Section II-B. For simplicity, we first discuss in detail the case of anti-extensive idempotent operators (i.e., openings and thinnings). Then, we extend the obtained results to the extensive counterpart (i.e., closings and thickenings).

A. Attribute Profiles

The definition of an *attribute opening profile* is quite straightforward since a sequence of attribute openings with a family of increasing criteria $T = \{T_\lambda : \lambda = 0, \ldots, n\}$, with $T_0 =$ true $\forall X \subseteq E$, leads to a granulometry. Thus, attribute opening profiles can be mathematically defined as

$$\Pi_{\gamma^T}(f) = \left\{\Pi_{\gamma^{T_\lambda}} : \Pi_{\gamma^{T_\lambda}} = \gamma^{T_\lambda}(f), \forall \lambda \in [0, \ldots, n]\right\}. \quad (16)$$

As for an MP, when $\lambda = 0$, $\Pi_{\gamma^{T_0}}(f) = \gamma^{T_0}(f) = f$. We point out that this definition of attribute opening profile includes also the morphological opening profile by reconstruction, since openings by reconstruction are a particular set of attribute openings. By comparing attribute profiles to conventional MPs, it can be noticed that both perform multiscale analysis of the image, since the SE/criterion, driven by the increasing scalar λ, progressively erases from the image larger structures. Moreover, attribute opening profiles provide the same capabilities in processing the image as for openings by reconstruction, but adding more flexibility in the definition of the filtering criterion. For example, if we consider a compact SE (e.g., square-,

[2]A MATLAB application that implements the proposed attribute profiles is available on request.

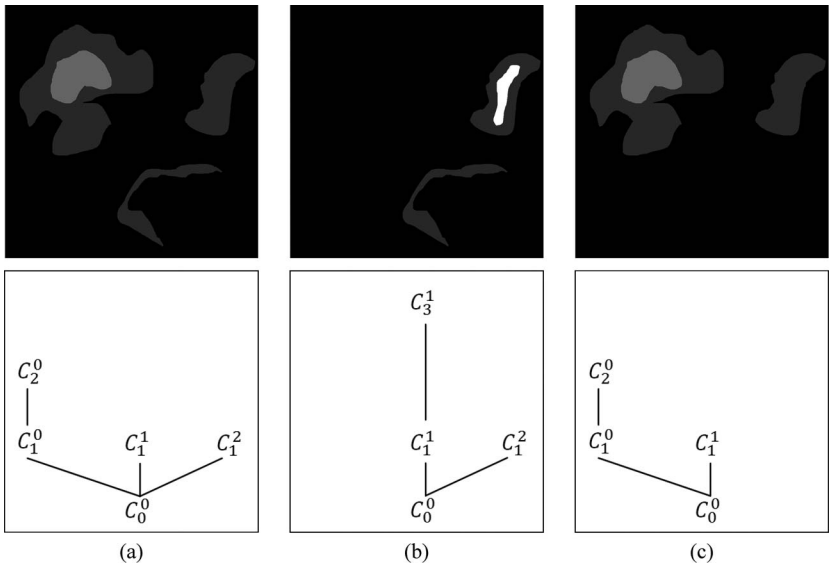

Fig. 2. Examples of attribute filtering on the image of Fig. 1(a). The first row reports the obtained filtered images, the second row the correspondent pruned Max-tree. Criterion: (a) "area $>$ 20 000"; b) "moment of inertia $>$ 0.25" and (c) "standard deviation $>$ 0."

disk-shaped), the structures are removed from the scene if the SE does not fit in them. Thus, the image is processed according to the smallest size of the regions. If we consider instead the length of the diagonal of the box bounding each region as an attribute, then, the structures are filtered according to a measure of their global extension, which is still related to the concept of scale, but in a different way with respect to considering the smallest size of the objects. Moreover, if we take into account the area of the regions, a different measure of the size of the objects is provided. Thus, by selecting different type of attributes, even if they are all increasing measures, different characterizations of the scale of the structures are generated.

If we consider other types of attributes not constrained by the increasingness property, a different behavior is achieved by the filters. For instance, it is possible to assess how the image reacts to a filtering done on multiple levels with an attribute invariant to changes in scale. This would permit to characterize the image by extracting information related to the shape of the structures through a measure which is independent of their size [21]. Thus, the application of attribute thinning in a multilevel approach leads to *attribute thinning profiles*. However, their definition is not direct as for attribute opening profiles. In fact, since attribute thinnings are not increasing, the absorption law might not be satisfied in the profile. This can result in sequential elements of the profile that are not ordered. For example, regions erased at a certain level of the profile might appear again in subsequent levels associated to more relaxed criteria. This is an undesirable effect particularly if a derivative of the profile needs to be computed. In order to build a consistent profile on attribute thinnings, it is necessary that the absorption law is fulfilled by the filtered images, leading the AP to be a set of cumulative functions. This can be obtained by constraining the criteria used in the filtering. The family of non-increasing criteria $U = \{U_\lambda : \lambda = 0, \ldots, n\}$ considered for computing the profile *has to be an ordered set*. Moreover, the criteria have to be consistently either in the form of $U_\lambda = a(X) > \tau_\lambda$ or $U_\lambda = a(X) < \tau_\lambda$ for all the connected component $X \subseteq E$, and $\tau_i \leq \tau_j$ for $i \leq j$, with a denoting a generic non-increasing attribute computed on the component X, and τ_λ being the scalar value taken as the threshold at the level λ of the profile. If the criteria are ordered and defined as mentioned above, then the following rule holds: If a connected set $X \subseteq E$ does not satisfy the criterion U_i (i.e., $U_i(X) = false$), then also $U_j(X) = false$, with $i \leq j$ and $U_i,\ U_j \in U$. Thus, for binary trivial thinning, it holds that if $\tilde{\Gamma}_{U_i}(X) = \varnothing \Rightarrow \tilde{\Gamma}_{U_j}(X) = \varnothing$ and this leads $\tilde{\Gamma}^{U_i}(F) \subseteq \tilde{\Gamma}^{U_j}(F)$ for binary attribute thinning. In the grayscale case, it becomes $\tilde{\gamma}^{U_i}(f) \leq \tilde{\gamma}^{U_j}(f)$. The latter property corresponds to the absorption law that can be expresses also as $\tilde{\gamma}^{U_i}\tilde{\gamma}^{U_j}(f) = \tilde{\gamma}^{U_{\max(i,j)}}(f)$. Thus, by selecting these criteria, the profile is behaving like a granulometry.

Consequently, it is possible to define an attribute thinning profile, based on a set of ordered criteria $U = \{U_\lambda : \lambda = 0, \ldots, n\}$, with $U_0 = true\ \forall X \subseteq E$ as

$$\Pi_{\tilde{\gamma}^U}(f) = \left\{\Pi_{\tilde{\gamma}^{U_\lambda}} : \Pi_{\tilde{\gamma}^{U_\lambda}} = \tilde{\gamma}^{U_\lambda}(f), \forall \lambda \in [0, n]\right\}. \quad (17)$$

Actually $\Pi_{\tilde{\gamma}^U}$ includes also Π_{γ^T} in its definition since the attribute thinning profile produces the same results as for the attribute openings if the criteria U fulfill the more restrictive property of increasingness. By duality, the *attribute closing profile* can be defined as

$$\Pi_{\tilde{\phi}^U}(f) = \left\{\Pi_{\tilde{\phi}^{U_\lambda}} : \Pi_{\tilde{\phi}^{U_\lambda}} = \tilde{\phi}^{U_\lambda}(f), \forall \lambda \in [0, n]\right\} \quad (18)$$

and analogously to (3), we can define an *attribute profile* as (19), shown at the bottom of the next page. Attribute thinning profiles permit us to perform a multilevel analysis of the image based on attributes (represented by ordered criteria) not necessarily related to the scale of the structures of the image. In fact, the choice of attributes like the shape factor, the spatial moments, etc., results in an AP that represents a multilevel (not multiscale) decomposition of the image according only to the shape of the regions. Furthermore, the attribute can also be a

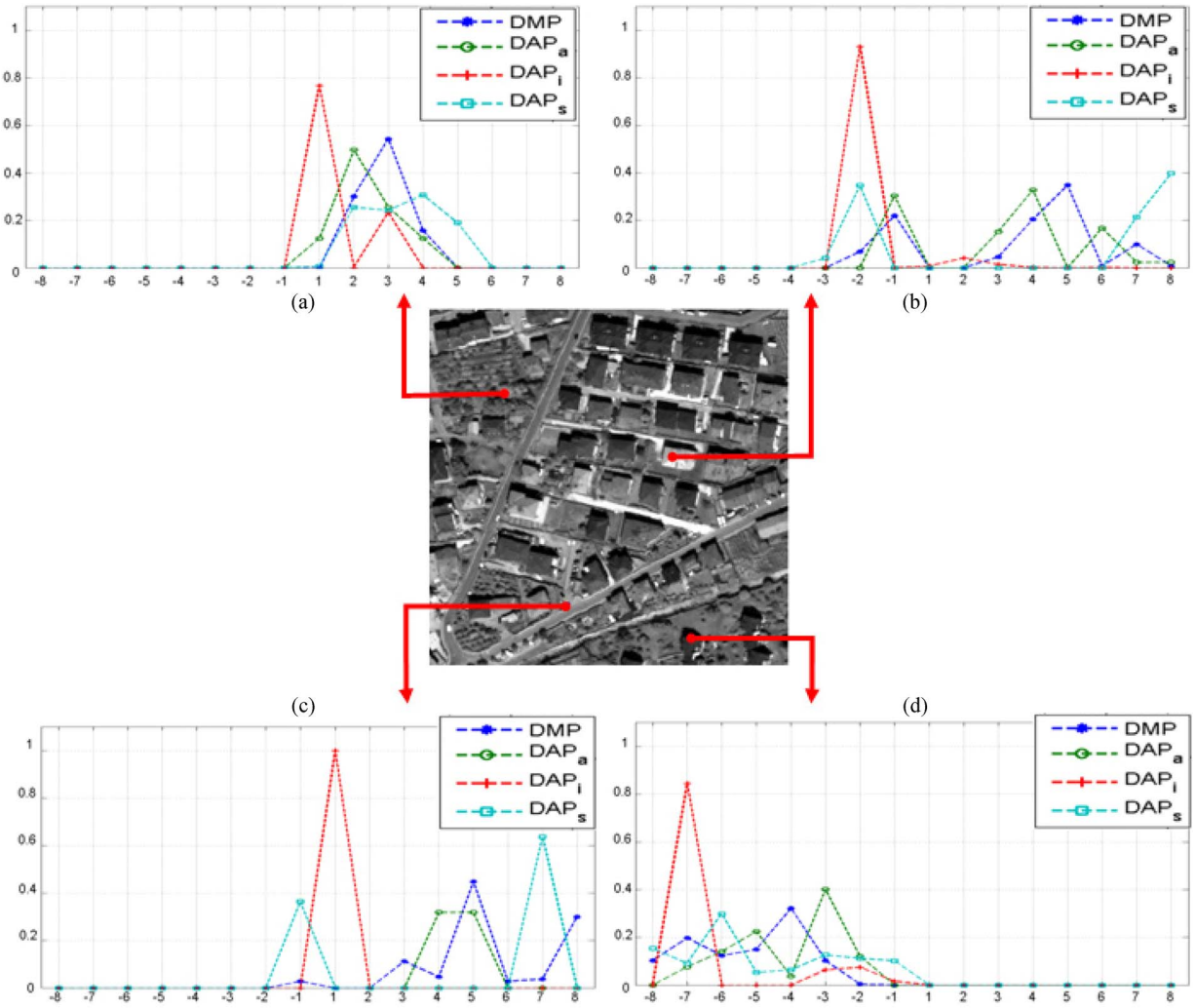

Fig. 3. Examples of four differential profiles computed on four samples belonging to different thematic classes (Vegetation, Road, Building, and Shadow) from a panchromatic Quickbird image of Trento (Italy). The values of the shown profiles are normalized in the range [0,1]. The horizontal axis reports the levels of the profiles. In the legend, DMP refers to the conventional DMP built by a squared-SE, DAP$_a$, DAP$_i$, DAP$_s$ denote the differential attribute profiles built on the area, moment of inertia, and standard deviation attribute, respectively. The subtractive rule was considered for the non-increasing criteria. (a) Vegetation. (b) Building. (c) Road. (d) Shadow.

measure which is not related to the geometry of the regions but to the graylevels of their pixels. For example, the scene can be simplified by removing structures according to homogeneity instead of their scale or shape.

As for MPs, the residuals of the progressive filtering can be important. Thus we can extend (4) by introducing the differential attribute profile for the set of non-increasing criteria U as (20), shown at the bottom of the page, where $\Delta_{\tilde{\phi}^{U_\lambda}}$ and $\Delta_{\tilde{\gamma}^{U_\lambda}}$ represent the differential thickening and thinning profiles, respectively, whose definition is straightforward and thus not reported.

Examples of a DMP and three DAPs computed on a panchromatic Quickbird image of the city of Trento (Italy) for four different thematic classes are presented in Fig. 3. The attributes selected for the three DAPs are: 1) area; 2) moment of inertia; and 3) standard deviation. By analyzing the differential profiles,

$$\Pi(f) = \left\{ \Pi_i : \left\langle \begin{array}{lll} \Pi_i = \Pi_{\tilde{\phi}^{U_\lambda}}, & \text{with } \lambda = (n-i+1), & \forall i \in [1,n] \\ \Pi_i = \Pi_{\tilde{\gamma}^{U_\lambda}}, & \text{with } \lambda = (i-n-1), & \forall i \in [n+1, 2n+1] \end{array} \right\} \right. \tag{19}$$

$$\Delta(f) = \left\{ \Delta_i : \left\langle \begin{array}{lll} \Delta_i = \Delta_{\tilde{\phi}^{U_\lambda}}, & \text{with } \lambda = (n-i+1), & \forall i \in [1,n] \\ \Delta_i = \Delta_{\tilde{\gamma}^{U_\lambda}}, & \text{with } \lambda = (i-n), & \forall i \in [n+1, 2n] \end{array} \right\} \right. \tag{20}$$

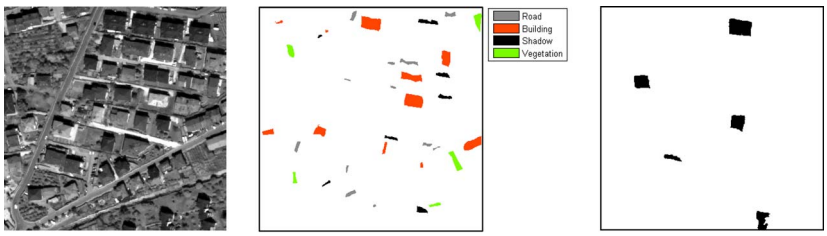

Fig. 4. Data set 1—(a) Panchromatic image of 400 × 400 pixels, (b) map of the test areas, and (c) map of the objects selected for the assessment of the geometrical accuracy.

as expected, it can be noticed that the DMP shows a similar behavior to the DAP with the area attribute, since both process shows the image according to the scale of the objects. The DAPs built on the moment of inertia and the standard deviation have a different behavior from the scale attributes. However, given a region, regardless of the type of attribute considered, the active responses of the pixels belonging to the region in the profile are all located either in the opening or closing part of the profile. In fact, dark objects are detected in the closing profile and bright ones on the opening side. The diversity shown by considering the DAPs built on different types of attributes results in features that potentially can increase in the separability of the information classes.

B. Analysis of the Complexity

The main advantage, in terms of computational complexity, of the approach based on the Max-tree, with respect to the use of operators by reconstruction for performing multilevel filtering, relies on the fact that the image has not to be completely processed at each level of the profile. In fact, the tree structure is built only once from the original image and after the attribute is computed on the components of the image, the same data structure is pruned by a set of thresholds λ, generating the filtered images at the different levels. Moreover, we point out that, if an attribute can be computed incrementally (e.g., area, volume, standard deviation, etc.), the computation of the attribute can be embedded in the creation of the tree, thus avoiding visiting all the nodes further. If a multilevel, multi-attribute analysis is performed, the processing can further take advantage from the architecture based on the Max-tree. In fact, the tree is still created only once, and the investigated attributes can be computed on the nodes, if possible, directly during the creation of the tree. However, even if the attributes need to be computed off-line after the creation of the tree, they can be calculated simultaneously at the visiting of each node, requiring a single scan of the tree. Moreover, during the computation of the attributes, their dependences can be exploited. For example, if the standard deviation and the area attributes need to be computed, the former requires in its definition the computation of the area, which can be directly exploited from the second attribute. Obviously, this further optimizes the analysis. Finally, the evaluation stage simply checks the criteria against the attributes values of the nodes in the tree. This is the only operation in the entire analysis that linearly depends on the number of levels and attributes considered.

If we quantitatively analyze the computational complexity of the implementation of the different operators, the conventional opening by reconstruction based on the iterative geodesic reconstruction [2] has a worst case time complexity with an upper bound of $O(N^2)$, where N is the number of pixels in the image. When computing a granulometry by reconstruction composed by L levels, the computational complexity has an order of $2LN^2$ in the worst case. Vincent [24] proposed an efficient algorithm based on first-input-first-output queue and two raster scans of the image which is an order of magnitude faster than the conventional technique and, thus, can reduce the load of computing a profile. Nevertheless, the image has to be entirely processed $2L$ times, regardless the algorithm considered. Instead, when considering an approach based on the Max-tree, the computational complexity of the analysis can be reduced. The most demanding stage of an attribute filtering based on the Max-tree is the creation of the tree that relies on a flood-filling algorithm. This algorithm is linear with respect to both the number of pixels and the connectivity [25]. The pruning of the tree and the image restitution are both $O(N)$ operations. Thus, the computational cost of a profile is $O(NG + 4LN)$, being G the number of graylevels in the image. On parallel machines, the Max-tree computation is further speeded up according to a slightly varying implementation based on the union-find algorithm [26]. More considerations on the memory use of Max-trees according to their implementation can be found in [25] and [26].

V. Experimental Analysis

A. Data Set Description

The experimental analysis was carried out by classifying two portions taken from a large VHR panchromatic image acquired by the Quickbird sensor on July 2006 with geometric resolution of 0.6 m. We did not consider the multispectral images acquired by the Quickbird scanner in order to focus the analysis only on the capabilities of different APs to model the geometrical/spatial information. This choice is also reasonable for some operational conditions when satellites that acquire only the panchromatic band (e.g., WorldView 1) are used.

The two considered images are made up by 400 × 400 [Fig. 4(a)] and 900 × 900 [Fig. 5(a)] pixels, respectively. Both the images represent two complex urban areas belonging to the city of Trento, Italy. Most of the surveyed buildings are residential with heterogeneous size and shape. Some large industrial buildings are also present in the scene. The presence of shadows

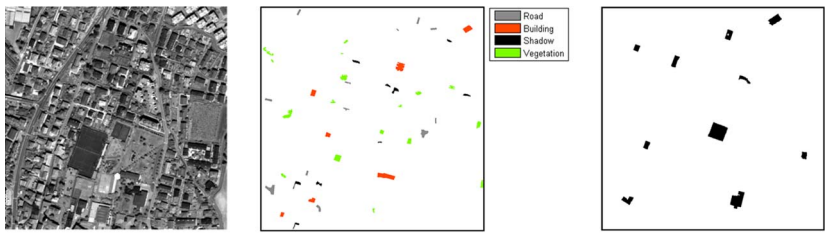

Fig. 5. Data set 2—(a) Panchromatic image of 900 × 900 pixels, (b) map of the test areas, and (c) map of the objects selected for the assessment of the geometrical accuracy.

TABLE I
NUMBER OF SAMPLES PER CLASS FOR THE TRAINING AND TEST SET FOR THE TWO DATA SETS

Land cover	Data set 1 (# of Samples)		Data set 2 (# of Samples)	
	Training	Test	Training	Test
Roads	199	907	300	3068
Buildings	209	3330	300	4184
Shadow	255	853	300	1715
Vegetation	222	1030	300	4568
Total	855	6120	1200	13535

can be observed particularly in proximities of buildings. All these factors contribute to the complexity of the considered scene.

The pixels of the two images were grouped into four informative classes: 1) Road; 2) Building; 3) Shadow; and 4) Vegetation. For both images, a training set, composed by samples randomly selected from labeled areas not included in the test sets, was considered and two independent test sets were defined by photo-interpretation in order to evaluate the performances of the classification. One test set is devoted to the evaluation of the thematic accuracy, while the other checks the geometric precision of the classification map on a set of selected objects in the scene according to the protocol proposed in [27] and [28]. The geometrical accuracy is evaluated by a set of five indexes modeling: 1) oversegmentation (OS); 2) undersegmentation (US); 3) fragmentation (FG); 4) shape factor (SH); and 5) errors on the objects borders (ED). The index modeling the OS gives a measure of the overlap between the region which mostly covers a reference objects in the classification map and the area of reference objects. The US error computes how much the regions correspondending to the reference objects are larger than the reference objects. The FR index refers to a descriptor of how the areas of the reference objects are fragmented in different regions in the classification map. Finally, the SH and the ED measures indicate how the shapes and the edges, respectively, of the reference objects differ to those of the correspondent regions in the reference map. All the error indexes range from zero to one (in the tables, the values are given in percentages), with zero representing a perfect match and one the greatest divergence between the reference objects and the correspondent regions in the classification map. For further information on the geometric error indexes, the reader can refer to [28]. The two test sets are reported in Fig. 4(b) and (c) and Fig. 5(b) and (c) for data set 1 and 2, respectively. The number of samples selected for training and testing the two data sets are reported in Table I.

B. Results

For both the images, a 17-D morphological profile was generated using a squared-SE with size increasing in eight steps (7, 13, 19, 25, 31, 37, 43, and 49). These values were arbitrarily chosen and since they range from 4.2 to 29.4 m, they are able to model the size of the heterogeneous objects in the scene. Three attribute profiles with the same dimensionality of the MP were also created following the approach based on the Max-tree data structure. All the filtering transformations were performed on the already constructed tree in order to reduce the computational burden. For all the APs, the considered criterion was "the attribute must be greater than λ."

Three different attributes were considered for the construction of the AP: 1) the area; 2) first moment of Hu; and 3) the standard deviation. The AP with the area attribute describes the scale of the structures in the scene; it is the only increasing attribute among the three selected. In order to create the profile with the area attribute, the following values of λ were selected: 49, 169, 361, 625, 961, 1369, 1849, and 2401. Although, these values correspond to the square of the SE sizes used for creating the MP, the multiscale analysis obtained models; the scale of the objects in the scene with a different criterion with respect to the MP. The second attribute considered is the moment of inertia. The original image was filtered by progressively suppressing from the scene those regions with attribute smaller than the following increasing thresholds: 0.2, 0.3, 0.4, 0.5, 0.6, 0.7, 0.8, and 0.9. The AP based on the standard deviation attribute performs a multilevel decomposition of the objects in the scene that is not related to the geometry of the regions but models the homogeneity of the graylevels of the pixels in the regions. The profile was built according to the following reference values of the standard deviation: 10, 20, 30, 40, 50, 60, 70, and 80. As for the definition of the SE sizes in the MP, the threshold values of λ were arbitrarily selected in order to cover the significant range of variation of the attribute for all the connected components of the image. Different analyses

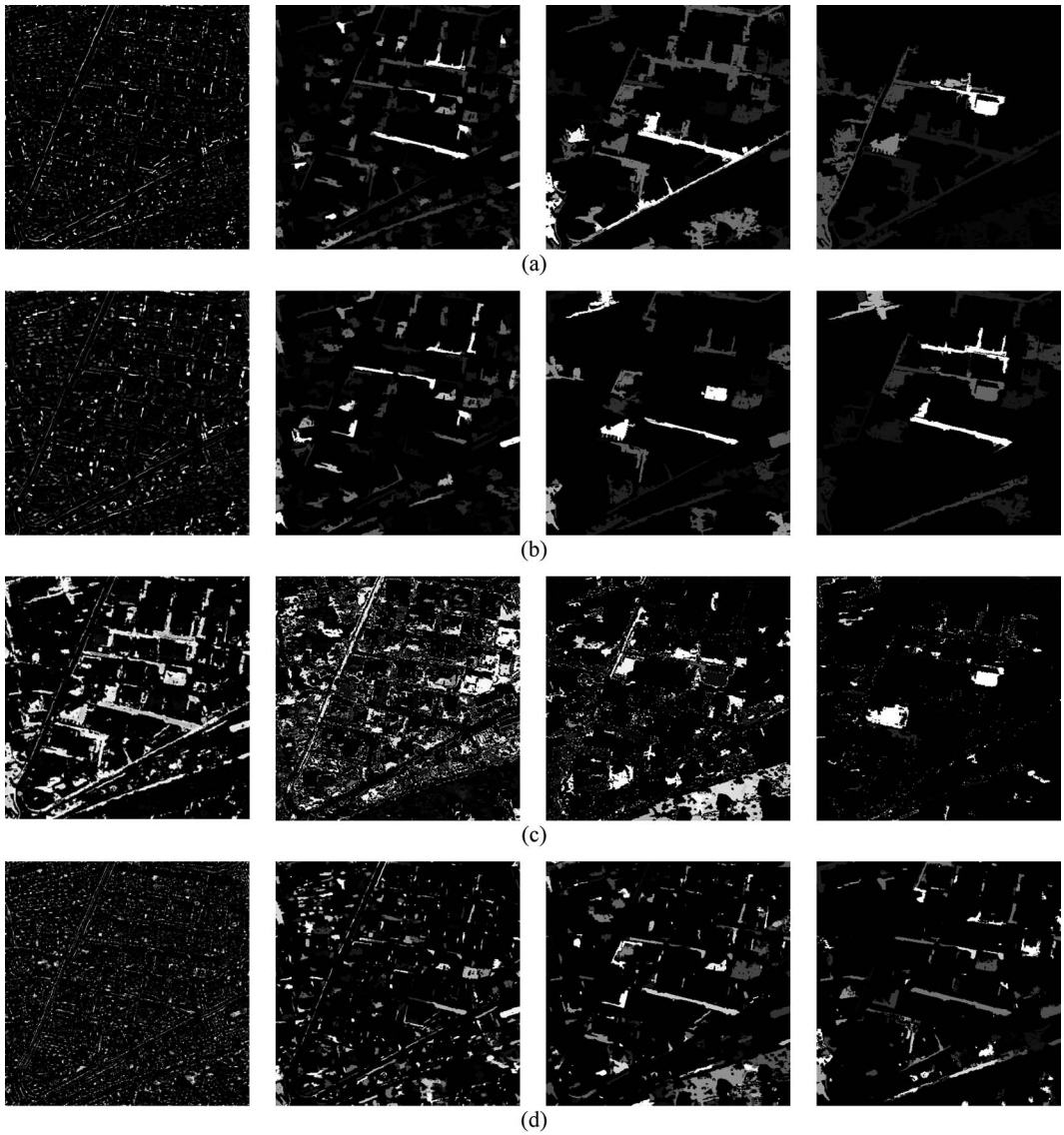

Fig. 6. Extracts of differential profiles built on the first data set. (a) DMP created by a SE with a square shape, DAPs with (b) area attribute, (c) moment of inertia attribute, and (d) standard deviation attribute. For all the profiles the levels one, three, five, and seven are reported from left to right. All the images are stretched for visual purposes.

were carried out on the data. At first, each AP was considered separately and then, all the features extracted by the APs were taken into account simultaneously.

In order to compare the behavior of the different profiles, we chose to present the derivatives of the constructed profiles (i.e., DMP and DAPs) because the differences among them are perceptually more visible than by analyzing the correspondent morphological/attribute profiles. The DMP [Fig. 6(a)] is visually similar to the DAP built by evaluating the area attribute [Fig. 6(b)]. Many regions, which are suppressed at a certain level in the DMP, are present at the same level in the DAP. However, some other objects are not revealed at the same level in the two profiles but in adjacent levels. For example, the thin and elongated region in the middle of the scene that is present in the second and third image from the left (levels three and five, respectively) in the DMP, in the DAP results in the third and fourth (respectively five and seven). These differences in the two differential profiles are mainly due to the different modeling of the concept of scale and to the choice done for the step size of the SEs and of the values of the thresholds λ, for the area attribute. In particular, the filters based on the area attribute remove the structures from the image according to their cardinality, whereas, the operators by reconstruction with a square SE interact to the smallest size of each region. Thus, this different behavior is particularly evident when considering elongated regions.

Different conclusions can be drawn by comparing the DMP to the DAPs generated by the moment of inertia and the standard deviation. At first, it is evident that at higher levels of the profiles (i.e., related to large values of λ), also regions that are spatially smaller than some others, appeared in previous levels, are present. This is due to the non-increasingness of the selected criterion.

In order to quantitatively compare the capabilities of the proposed profiles in modeling the spatial characteristics of the scene, we classified the original image using each profile.

TABLE II
ERRORS OBTAINED BY CLASSIFYING THE PANCHROMATIC IMAGE ALONG WITH MORPHOLOGICAL/ATTRIBUTE PROFILES FOR DATA SET 1

Features	Thematic Error Index		Geometric Error Indexes				
	Overall Error (%)	1-Kappa (%)	OS (%)	US (%)	ED (%)	FG (%)	SH (%)
PAN	46.5	63.9	40.6	21.9	61.9	18.8	18.7
MP	32.4	45.9	12.8	51.4	66.5	12.7	15.0
AP area	46.9	54.2	15.3	46.5	62.5	15.3	18.2
AP inertia	33.6	41.5	11.7	55.9	69.0	11.6	12.8
AP std	33.0	47.7	13.8	51.2	66.7	13.7	13.8
AP inertia + AP std	23.0	32.4	13.4	46.8	61.9	13.4	16.1
AP all	30.5	37.9	13.2	43.6	62.9	13.2	16.9

TABLE III
ERRORS OBTAINED BY CLASSIFYING THE PANCHROMATIC IMAGE ALONG WITH MORPHOLOGICAL/ATTRIBUTE PROFILES FOR DATA SET 2

Features	Thematic Error Index		Geometric Error Indexes				
	Overall Error (%)	1-Kappa (%)	OS (%)	US (%)	ED (%)	FG (%)	SH (%)
PAN	56.2	77.2	60.8	16.6	71.4	23.0	16.6
MP	39.9	56.4	44.8	18.1	50.9	3.4	15.0
AP area	52.4	73.4	44.3	12.7	61.7	13.9	15.7
AP inertia	40.5	56.8	15.8	71.4	82.9	4.9	20.9
AP std	41.1	57.9	34.6	52.0	70.7	11.0	15.8
AP inertia + AP std	28.1	39.1	27.0	44.2	62.4	10.3	16.4
AP all	28.3	39.4	27.7	46.3	64.9	15.2	15.5

TABLE IV
CLASS SPECIFIC PRODUCER ACCURACY (PA) AND USER ACCURACY (UA) OBTAINED BY CLASSIFYING THE PANCHROMATIC IMAGE ALONG WITH MORPHOLOGICAL/ATTRIBUTE PROFILES FOR DATA SET 1. THE BEST ACCURACIES OBTAINED ARE MARKED IN BOLD

Features	Road		Building		Shadow		Vegetation	
	PA (%)	UA (%)	PA (%)	UA (%)	PA (%)	UA (%)	PA (%)	UA (%)
PAN	29.5	62.1	76.1	42.4	94.0	97.1	32.0	45.7
MP	31.6	73.5	90.7	55.1	92.5	97.4	74.0	78.5
AP area	33.1	77.2	71.0	33.2	92.5	97.4	39.6	59.8
AP inertia	41.1	76.6	**93.9**	49.7	87.6	**97.5**	51.3	85.6
AP std	32.4	87.8	90.7	46.5	94.3	97.1	85.8	**90.0**
AP inertia + AP std	**96.6**	45.6	62.5	**96.8**	**98.0**	94.7	**89.1**	79.0
AP all	41.8	**89.5**	93.4	51.0	92.2	97.4	62.7	88.9

A random forest technique with 200 trees was used for the classification [29]. The random forest classifier is formed by an ensemble of decision tree classifiers. We chose to use this non-parametric classifier because of the high redundancy shown by the profiles that can be critical for the estimation of the statistics in classical parametric classifiers. The classification is achieved by selecting the output of the ensembles of the tree classifiers according to a majority voting. The features considered by the classifier were the panchromatic band and the generated profiles. For the definition of the split on each node in the random forest, the number of considered variables was correspondent to the square root of the number of input features. The aim of this analysis was to investigate how the accuracy (both thematic and geometric) varies when including in the analysis the knowledge gathered on the spatial domain by the profiles. In particular, the results obtained by considering the panchromatic band and a conventional MP were compared to those obtained by different APs.

Tables II and III show the thematic error index, in terms of percentage overall error and the kappa error (computed as 1-kappa coefficient in percentage) on the test set, and the five geometric error indexes. Furthermore, the accuracies obtained by each class are shown in Tables IV and V. In particular, the producer and user accuracy are reported. We recall that the PA is computed, for each class, as the total number of the patterns correctly classified divided by the total number of the patterns belonging to the considered class in the reference map. The PA measures how many reference patterns are correctly classified by each class. The UA is obtained by dividing the total number of correctly classified patterns for each class by the total number of patterns classified to the same class. The UA indicates how many samples associated to a class are actually belonging to that class in the reference. More information on PA and UA can be found in [30].

By analyzing the thematic accuracies reported in Table II for the original panchromatic band, one can observe that a clear increase of the accuracy is obtained by using jointly the features that model the spatial information. The accuracy achieved by considering the MP is comparable to the one obtained by the single APs with moment of inertia and standard

TABLE V
CLASS SPECIFIC PRODUCER ACCURACY (PA) AND USER ACCURACY (UA) OBTAINED BY CLASSIFYING THE PANCHROMATIC IMAGE ALONG WITH MORPHOLOGICAL/ATTRIBUTE PROFILES FOR DATA SET 2. THE BEST ACCURACIES OBTAINED ARE MARKED IN BOLD

Features	Road		Building		Shadow		Vegetation	
	PA (%)	UA (%)	PA (%)	UA (%)	PA (%)	UA (%)	PA (%)	UA (%)
PAN	39.8	47.7	34.0	29.3	85.8	90.3	38.1	37.0
MP	60.2	22.6	67.2	52.7	88.6	**94.3**	49.8	79.3
AP area	60.4	40.7	33.4	25.1	89.4	93.4	38.9	55.7
AP inertia	87.4	69.5	56.9	11.6	87.1	92.2	45.8	**84.4**
AP std	68.0	15.1	51.5	**71.1**	86.6	94.1	56.1	64.1
AP inertia + AP std	69.2	**91.1**	66.5	69.8	**93.2**	86.7	**70.6**	60.1
AP all	**92.2**	69.9	**70.8**	60.1	88.1	93.8	59.0	75.2

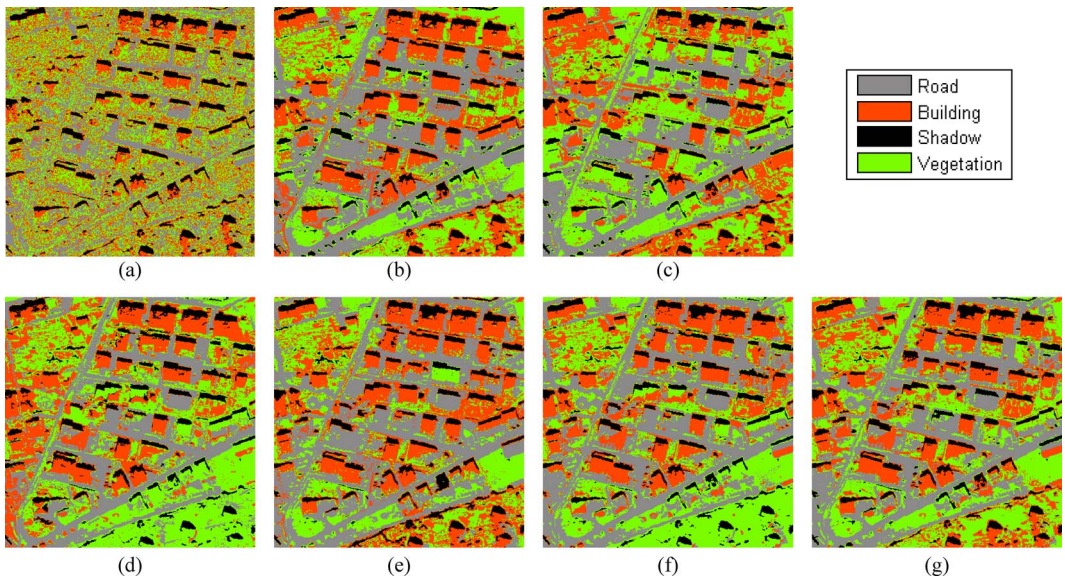

Fig. 7. Data set 1. Classification maps obtained by (a) panchromatic image only, (b) MP, (c) AP area, (d) AP inertia, (e) AP std, (f) AP inertia + AP std, and (g) AP all.

deviation attributes. Instead, the AP constructed on the area attribute produced the highest overall error and kappa error among the profiles. This is due to the selected thresholds used for computing the filtering, which might not properly model the great variety in the scale of the objects for the considered scene. The best results, according to the thematic accuracy, are obtained by the joint use of the AP with moment of inertia and the AP with standard deviation attribute, which reduced the overall classification error by about 24% and the kappa error of 32%, with respect to the use of the only original panchromatic image. The improvement was about 9% in overall error and 14% in kappa error, with respect to the conventional MP. Even if the global accuracies are in general quite small, making more complex the visual interpretation of the maps, by evaluating the geometric indexes, one can see that the classification of the panchromatic image shows a large oversegmentation error (thus, a small undersegmentation error) with respect to the maps obtained by considering the profiles. This behavior is also confirmed by a visual inspection of the classification maps shown in Fig. 7. In fact, it is possible to observe that the classification map obtained with the panchromatic image [Fig. 7(a)] is highly fragmented, whereas, the other maps are more homogeneous. As best case, when considering the map obtained by the AP with moment of inertia, a reduction by about 29% and 7% in the oversegmentation and fragmentation error, respectively, is achieved. This effect can be noticed in the row of buildings at the top of the image. Nevertheless, the AP inertia shows a high US error which can be due to the missed recognition of the buildings on the bottom of the image and the generation of broad areas. The lowest US error among the profiles and the overall lowest ED error are achieved, by considering the AP with moment of inertia and the AP with standard deviation attribute together.

Table III shows the error rates on the test set obtained by analyzing the data set 2. As for the previous data set, the thematic errors decrease when considering the spatial information provided by the profiles. Also, in this case, the results obtained by considering a single AP are similar to those generated by the MP (this is also clear from the classification maps in Fig. 8). In this experiment, the AP built on the area attribute results in a thematic error only slightly smaller than the one of the original panchromatic image (about 4% in both overall and kappa errors). However, as confirmed by the map, the geometrical errors are similar with those obtained by considering the other profiles. Again, the highest thematic accuracy is obtained when considering the APs with moment of inertia and standard deviation attributes. The thematic errors are reduced by about 28% in the overall error and 38% in kappa errors with respect to the original panchromatic image and by about 12% and 17% (overall and kappa errors) against

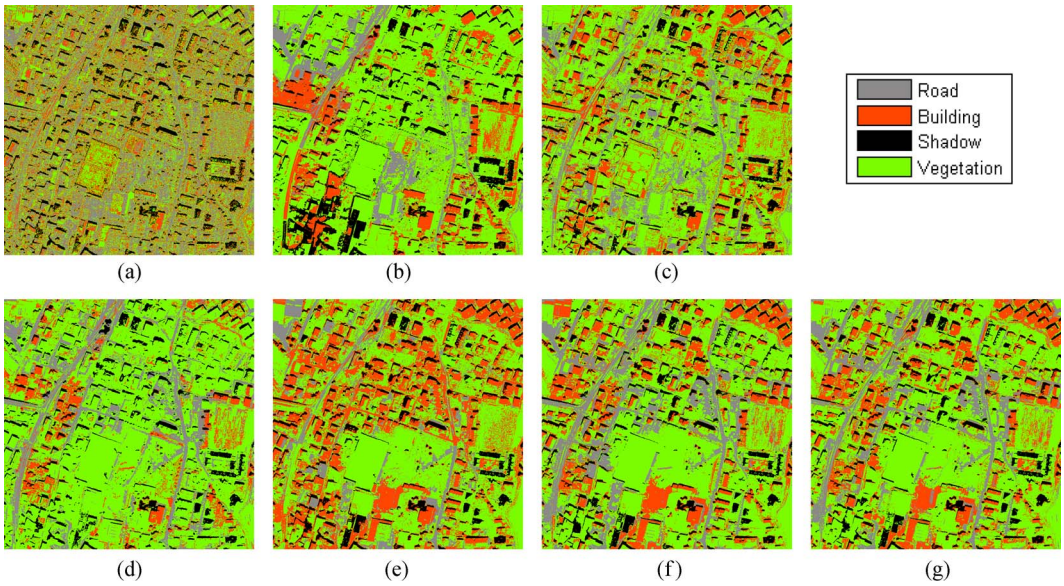

Fig. 8. Data set 2. (a) Panchromatic band; classification maps obtained by (b) MP, (c) AP area, (d) AP inertia, (e) AP std, (f) AP inertia + AP std, and (g) AP all.

the conventional MP. As for the first data set, better accuracies are obtained by considering only the AP with moment of inertia and the AP with standard deviation attribute than considering together also the AP with area attribute. This can be due to the increase in the dimensionality of the feature space given by considering also the AP with area attribute, which makes the analysis more complex (i.e., Hughes phenomenon), without providing enough additional independent information than to the other APs. However, one should observe that the selection of the threshold values λs affects the capability of the computed profile in modeling the spatial features of the objects. Thus, an AP with different threshold values for the area attribute might provide features which are more discriminant.

In addition, also the geometry of the reference objects is globally more precisely preserved by the AP with moment of inertia and AP with standard deviation attribute considered together in comparison to the other single profiles. In particular, the oversegmentation error in the map obtained by considering all the APs decreases of about 34% and 18%, compared to that of the map generated by the only panchromatic image and by the MP, respectively. This can be observed as a more uniform classification of the vegetated areas in the middle of the image and of some roads. As for data set 1, the AP inertia shows small US and FG errors but high US error, which can be due to the presence of large areas associated to the Vegetation class.

By considering Tables IV and V, it is possible to make a detailed class-by-class analysis by considering the producer accuracy (PA) and user accuracy (UA) obtained. The two results for both the data sets are analyzed together in order to observe trends in the obtained results. Focusing the attention on the specific thematic classes, we can underline as, with respect to the other attributes, the AP with moment of inertia performed well in identifying the roads, in particular for data set 2. However, for both data sets, the best results were obtained by considering all the APs. When considering the Building class, the conventional MP, the AP with standard deviation attribute, and the AP with all the attributes performed the best and gave comparable results. For this particular class, good results were also obtained by the AP with moment of inertia but only in data set 1. The class Shadow was globally well-classified by all the profiles and no particular trend in the results was noticed. Finally, the vegetated areas were extracted well by the AP with the standard deviation attribute particualrly in data set 1. The MP and the AP with moment of inertia and the one with all the attributes also reached similar results.

VI. Conclusion

In this paper, attribute profiles have been introduced for classification of very high resolution remote sensing images and differential attribute profiles have been proposed and formally defined. The motivation of this work relies on the need to improve the flexibility, the capability of modeling different kind of objects, and the computational load associated with the widely used conventional morphological profiles and their derivative.

Attribute profiles can be used for extracting information from the spatial domain by reducing the limitations of the morphological profiles. This approach allows one to analyze the original image in a multilevel fashion by the application of a sequence of morphological attribute operators. These operators are adaptive morphological connected filters, which include in their general definition also opening and closing by reconstruction. Attribute filters are flexible tools that enable to analyze an image, not only on the basis of the scale of the structures (as for operators by reconstruction), but also according to other measures/attributes computed on the regions. Thus, it is possible to perform a multilevel analysis of the scene by exploiting measures related to many different geometric primitives (e.g., shape), the graylevel of the pixels, or any other parameter that can be computed on the regions.

In the paper, we propose to compute the attribute profiles according to an effective implementation based on the Max-tree,

i.e., an efficient representation of the data, which leads to a reduction of the computational load of about one order of magnitude with respect to morphological profiles.

The proposed technique was applied to two very high resolution panchromatic images acquired by Quickbird satellite on the city of Trento, Italy. Three attribute profiles, based on different attributes, were extracted from the panchromatic band. We considered 1) the area (which is related to the MP created with a squared SE); 2) the moment of inertia (which is a descriptor of the geometry of a region invariant to the scale); and 3) the standard deviation of the graylevels of the pixels (which measures the homogeneity of the regions). The data were classified by a random forest classifier. The obtained maps were evaluated by checking their thematic accuracy and the geometric precision in representing some reference objects in the scene. The results pointed out the effectiveness of the proposed APs, which involved a sharply higher thematic and geometric accuracy with respect to considering the only panchromatic band. Moreover, the profiles built on different attributes led to similar results in terms of accuracy, but also conveyed different and complementary information into the classification process. In fact, the joint use of the three attribute profiles in the classification tasks resulted in an decrease of the classification kappa errors up to 38% and 17% with respect to the only panchromatic image and to the MP, respectively. The obtained classification maps are also more precise in the representation of the geometry of the regions as proven by the geometrical error indexes.

As future developments, we plan to investigate in depth the capabilities of APs and DAPs in the analysis of very high resolution images particularly for applications where the extraction of the spatial information has a fundamental role, such as the extraction and characterization of the objects in the scene. Moreover, it would be very interesting to analyze how the modeling of many different geometrical features can improve the analysis of multitemporal image series (e.g., for change detection task) particularly for urban areas.

ACKNOWLEDGMENT

This work was supported in part by the Research Fund of the University of Iceland and of the University of Trento.

REFERENCES

[1] F. Dell'Acqua, P. Gamba, A. Ferari, J. A. Palmason, J. A. Benediktsson, and K. Arnason, "Exploiting spectral and spatial information in hyperspectral urban data with high resolution," *IEEE Geosci. Remote Sens. Lett.*, vol. 1, no. 4, pp. 322–326, Oct. 2004.

[2] P. Soille, *Morphological Image Analysis, Principles and Applications*, 2nd ed. Berlin, Germany: Springer-Verlag, 2003.

[3] M. Pesaresi and J. A. Benediktsson, "A new approach for the morphological segmentation of high-resolution satellite imagery," *IEEE Trans. Geosci. Remote Sens.*, vol. 39, no. 2, pp. 309–320, Feb. 2001.

[4] M. Chini, N. Pierdicca, and W. Emery, "Exploiting SAR and VHR optical images to quantify damage caused by the 2003 Bam earthquake," *IEEE Trans. Geosci. Remote Sens.*, vol. 47, no. 1, pp. 145–152, Jan. 2009.

[5] D. Tuia, F. Pacifici, M. Kanevski, and W. Emery, "Classification of very high spatial resolution imagery using mathematical morphology and support vector machines," *IEEE Trans. Geosci. Remote Sens.*, vol. 47, no. 11, pp. 3866–3879, Nov. 2009.

[6] H. Akcay and S. Aksoy, "Automatic detection of geospatial objects using multiple hierarchical segmentations," *IEEE Trans. Geosci. Remote Sens.*, vol. 46, no. 7, pp. 2097–2111, Jul. 2008.

[7] J. Chanussot, J. Benediktsson, and M. Fauvel, "Classification of remote sensing images from urban areas using a fuzzy possibilistic model," *IEEE Geosci. Remote Sens. Lett.*, vol. 3, no. 1, pp. 40–44, Jan. 2006.

[8] J. A. Benediktsson, M. Pesaresi, and K. Arnason, "Classification and feature extraction for remote sensing images from urban areas based on morphological transformations," *IEEE Trans. Geosci. Remote Sens.*, vol. 41, no. 9, pp. 1940–1949, Sep. 2003.

[9] J. A. Benediktsson, J. A. Palmason, and J. R. Sveinsson, "Classification of hyperspectral data from urban areas based on extended morphological profiles," *IEEE Trans. Geosci. Remote Sens.*, vol. 43, no. 3, pp. 480–491, Mar. 2005.

[10] M. Fauvel, J. Benediktsson, J. Chanussot, and J. Sveinsson, "Spectral and spatial classification of hyperspectral data using SVMs and morphological profiles," *IEEE Trans. Geosci. Remote Sens.*, vol. 46, no. 11, pp. 3804–3814, Nov. 2008.

[11] R. Bellens, S. Gautama, L. Martinez-Fonte, W. Philips, J. C.-W. Chan, and F. Canters, "Improved classification of VHR images of urban areas using directional morphological profiles," *IEEE Trans. Geosci. Remote Sens.*, vol. 46, no. 10, pp. 2803–2813, Oct. 2008.

[12] P. Soille and M. Pesaresi, "Advances in mathematical morphology applied to geoscience and remote sensing," *IEEE Trans. Geosci. Remote Sens.*, vol. 40, no. 9, pp. 2042–2055, Sep. 2002.

[13] M. Dalla Mura, J. A. Benediktsson, F. Bovolo, and L. Bruzzone, "An unsupervised technique based on morphological filters for change detection in very high resolution images," *IEEE Geosci. Remote Sens. Lett.*, vol. 5, no. 3, pp. 433–437, Jul. 2008.

[14] M. Dalla Mura, J. A. Benediktsson, B. Waske, and L. Bruzzone, "Morphological attribute filters for the analysis of very high resolution images," in *Proc. IEEE IGARSS*, Cape Town, South Africa, Jul. 12–19, 2009, vol. III, pp. 97–100.

[15] M. Dalla Mura, J. A. Benediktsson, and L. Bruzzone, "Modeling structural information for building extraction with morphological attribute filters," in *Proc. SPIE Eur. Remote Sens.*, Berlin, Germany, Aug. 31–Sep. 3, 2009, p. 747 703.

[16] E. J. Breen and R. Jones, "Attribute openings, thinnings and granulometries," *Comput. Vis. Image Underst.*, vol. 64, no. 3, pp. 377–389, Nov. 1996.

[17] G. Matheron, *Random Sets and Integral Geometry*. Hoboken, NJ: Wiley, 1975.

[18] J. Serra, "Connectivity on complete lattices," *J. Math. Imaging Vis.*, vol. 9, no. 3, pp. 231–251, Nov. 1998.

[19] P. Salembier, A. Oliveras, and L. Garrido, "Anti-extensive connected operators for image and sequence processing," *IEEE Trans. Image Process.*, vol. 7, no. 4, pp. 555–570, Apr. 1998.

[20] E. R. Urbach and M. H. F. Wilkinson, "Shape-only granulometries and grey-scale shape filters," in *Proc. ISMM*, 2002, pp. 305–314.

[21] E. R. Urbach, J. B. T. M. Roerdink, and M. H. F. Wilkinson, "Connected shape-size pattern spectra for rotation and scale-invariant classification of gray-scale images," *IEEE Trans. Pattern. Anal. Mach. Intell.*, vol. 29, no. 2, pp. 272–285, Feb. 2007.

[22] M. K. Hu, "Visual pattern recognition by moment invariants," *IRE Trans. Inf. Theory*, vol. IT-8, no. 2, pp. 179–187, Feb. 1962.

[23] R. C. Gonzalez and R. E. Woods, *Digital Image Processing*, 3rd ed. Englewood Cliffs, NJ: Prentice-Hall, 2008.

[24] L. Vincent, "Morphological grayscale reconstruction in image analysis: Applications and efficient algorithms," *IEEE Trans. Image Process.*, vol. 2, no. 2, pp. 176–201, Apr. 1993.

[25] A. Meijster and M. H. F. Wilkinson, "A comparison of algorithms for connected set openings and closings," *IEEE Trans. Pattern Anal. Mach. Intell.*, vol. 24, no. 4, pp. 484–494, Apr. 2002.

[26] M. H. F. Wilkinson, H. Gao, W. H. Hesselink, J. E. Jonker, and A. Meijster, "Concurrent computation of attribute filters on shared memory parallel machines," *IEEE Trans. Pattern Anal. Mach. Intell.*, vol. 30, no. 10, pp. 1800–1813, Oct. 2008.

[27] L. Bruzzone and C. Persello, "A novel protocol for accuracy assessment in classification of very high resolution multispectral and SAR images," in *Proc. IGARSS*, 2008, vol. 2, pp. 265–268.

[28] C. Persello and L. Bruzzone, "A novel protocol for accuracy assessment in classification of very high resolution images," *IEEE Trans. Geosci. Remote Sens.*, vol. 48, no. 3, pp. 1232–1244, Mar. 2010.

[29] L. Breiman, "Random forests," *Mach. Learn.*, vol. 45, no. 1, pp. 5–32, Oct. 2001.

[30] R. G. Congalton and K. Green, *Assessing the Accuracy of Remotely Sensed Data: Principles and Practices*, 2nd ed. Boca Raton, FL: CRC Press, 2008.

Mauro Dalla Mura (S'08) received the B.S. (Laurea) and M.S. (Laurea Specialistica) degrees in telecommunication engineering from the University of Trento, Trento, Italy, in 2005 and 2007, respectively. He is currently working toward the Ph.D. jointly between the University of Trento and the University of Iceland, Reykjavik, Iceland.

Since 2007, he has been with the Remote Sensing Group at the Department of Information Engineering and Computer Science, University of Trento and with the Faculty of Electrical and Computer Engineering, University of Iceland, Reykjavik, Iceland. His main research activities are in the fields of remote sensing, image processing, and pattern recognition. In particular, his interests include mathematical morphology, classification, and change detection.

Mr. Dalla Mura is a Reviewer for the IEEE TRANSACTIONS ON GEOSCIENCE AND REMOTE SENSING and the *Canadian Journal of Remote Sensing*.

Jón Atli Benediktsson (S'84–M'90–SM'99–F'04) received the Cand.Sci. degree in electrical engineering from the University of Iceland, Reykjavik, Iceland, in 1984, and the M.S.E.E. and Ph.D. degrees from Purdue University, West Lafayette, IN, in 1987 and 1990, respectively.

He is currently Pro Rector for academic affairs and a Professor of electrical and computer engineering with the University of Iceland. He has held visiting positions with the Department of Information and Communication Technology, University of Trento, Trento, Italy, since 2002; the School of Computing and Information Systems, Kingston University, Kingston upon Thames, U.K., during 1999 to 2004; the Joint Research Centre of the European Commission, Ispra, Italy, in 1998; the Technical University of Denmark, Lyngby, Denmark, in 1998; and the School of Electrical and Computer Engineering, Purdue University, in 1995. In August 1997, he was a Fellow with the Australian Defence Force Academy, Canberra, A.C.T., Australia. From 1999 to 2004, he was the Chairman of the energy company Metan Ltd. He was also the Chairman of the University of Iceland's Science and Research Committee from 1999 to 2005. Since 2006, he has been the Chairman of the University of Iceland's Quality Assurance Committee. He coedited (with Prof. D. A. Landgrebe) a Special Issue on Data Fusion of the IEEE TRANSACTIONS ON GEOSCIENCE AND REMOTE SENSING (TGRS) (May 1999) and (with P. Gamba and G. G. Wilkinson) a Special Issue on Urban Remote Sensing from Satellite (October 2003). His research interests include remote sensing, pattern recognition, machine learning, image processing, biomedical engineering, and signal processing, and he has published extensively in those fields.

Dr. Benediktsson is a member of Societas Scinetiarum Islandica and Tau Beta Pi. He was the Past Editor and is currently Associate Editor for TGRS and Associate Editor for the IEEE GEOSCIENCE AND REMOTE SENSING LETTERS. From 1999 to 2002, prior to being Editor, he was Associate Editor for TGRS. From 1996 to 1999, he was the Chairman of the IEEE Geoscience and Remote Sensing Society (GRSS) Technical Committee on Data Fusion and was elected to the Administrative Committee of the GRSS for the terms 2000 to 2002 and 2008 to 2010. He is currently, the Executive Vice President of GRSS. In 2002, he was appointed as Vice President of Technical Activities of GRSS, and in 2008, he was appointed as Vice President of Professional Activities of GRSS. He was the founding Chairman of the IEEE Iceland Section and served as its Chairman from 2000 to 2003. He was a member of a NATO Advisory Panel of the Physical and Engineering Science and Technology Subprogram (2002–2003). He was a member of Iceland's Science and Technology Council (2003–2006) and a member of the Nordic Research Policy Council (2004). He received the Stevan J. Kristof Award from Purdue University, in 1991, as an outstanding graduate student in remote sensing. In 1997, he was the recipient of the Icelandic Research Council's Outstanding Young Researcher Award. In 2000, he was granted the IEEE Third Millennium Medal. In 2004, he was a corecipient of the University of Iceland's Technology Innovation Award. In 2006, he received the yearly research award from the Engineering Research Institute, University of Iceland. In 2007, he received the Outstanding Service Award from the IEEE GRSS.

Björn Waske (S'06–M'08) received the M.Sc. degree in applied environmental sciences with a major in remote sensing from the University of Trier, Trier, Germany, in 2002 and the Ph.D. degree from the University of Bonn, Bonn, Germany, in 2007.

From 2004 to 2007, he was with the Center of Remote Sensing of Land Surfaces (ZFL), University of Bonn and visited the Department of Electrical and Computer Engineering, University of Iceland, Reykjavik, Iceland for three months in 2006. Until mid-2004, he was a Research Assistant with the Department of Geosciences, Munich University, Munich, Germany, where he worked on the use of remote sensing data for flood forecast modeling. Since September 2009, he has been an Assistant Professor at the Institute of Geodesy and Geoinformation, Faculty of Agriculture, University of Bonn. His current research interests include advanced concepts for image classification and data fusion, focusing on multisensor applications.

Dr. Waske is a Reviewer for the IEEE TRANSACTIONS ON GEOSCIENCE AND REMOTE SENSING and the IEEE GEOSCIENCE AND REMOTE SENSING LETTERS.

Lorenzo Bruzzone (S'95–M'98–SM'03–F'10) received the M.S. (Laurea) degree in electronic engineering (*summa cum laude*) and the Ph.D. degree in telecommunications from the University of Genoa, Genoa, Italy, in 1993 and 1998, respectively.

He his currently a Full Professor of telecommunications at the University of Trento, Trento, Italy, where he teaches remote sensing, pattern recognition, radar, and electrical communications. He is the Head of the Remote Sensing Laboratory in the Department of Information Engineering and Computer Science, University of Trento. His current research interests are in the areas of remote sensing, signal processing, and pattern recognition (analysis of multitemporal images; feature extraction and selection; classification, regression, and estimation; data fusion; and machine learning). In 2008, was appointed as a member of the joint NASA/ESA Science Definition Team for *Outer Planet Flagship Missions*. He is the author (or coauthor) of 90 scientific publications in referred international journals (61 in IEEE journals), more than 140 papers in conference proceedings, and 13 book chapters. He is the Editor/Co-editor of 10 books/conference proceedings. He is a Referee for many international journals and has served on the Scientific Committees of several international conferences. He conducts and supervises research on these topics within the frameworks of several national and international projects.

Dr. Bruzzone is a member of the Managing Committee of the Italian Inter-University Consortium on Telecommunications and a member of the Scientific Committee of the India–Italy Center for Advanced Research. He is also a member of the International Association for Pattern Recognition and of the Italian Association for Remote Sensing (AIT). Since 2009, he has been a member of the Administrative Committee of the IEEE Geoscience and Remote Sensing Society. He was the General Chair and Co-chair of the First and Second IEEE International Workshop on the Analysis of Multi-temporal Remote-Sensing Images (MultiTemp), and is currently a member of the Permanent Steering Committee of this series of workshops. Since 2003, he has been the Chair of the SPIE Conference on Image and Signal Processing for Remote Sensing. From 2004 to 2006, he served as an Associated Editor of the IEEE GEOSCIENCE AND REMOTE SENSING LETTERS, and currently is an Associate Editor for the IEEE TRANSACTIONS ON GEOSCIENCE AND REMOTE SENSING (TGRS) and the *Canadian Journal of Remote Sensing*. He ranked first place in the Student Prize Paper Competition of the 1998 IEEE International Geoscience and Remote Sensing Symposium (Seattle, July 1998). He was a recipient of the Recognition of IEEE TGRS Best Reviewers in 1999 and was a Guest Co-Editor of different Special Issues of the IEEE TGRS.